Supporting Information

Wearable Textile Battery Rechargeable by Solar Energy

Yong-Hee Lee,[†,§] *Joo-Seong Kim,*[†,§] *Jonghyeon Noh,*[†,§] *Inhwa Lee,*[‡] *Hyeong Jun Kim,*[‡] *Sunghun Choi,*[†] *Jeongmin Seo,*[‡] *Seokwoo Jeon,*[⊥,∥] *Taek-Soo Kim,*[*,‡,∥] *Jung-Yong Lee,*[*,†,∥] *Jang Wook Choi*[*,†,∥]

[†]Graduate School of EEWS (WCU), [‡]Department of Mechanical Engineering, [⊥]Department of Materials Science and Engineering, [∥]KAIST Institute NanoCentury, Korea Advanced Institute of Science and Technology (KAIST), Daejeon 305-701, Republic of Korea

[§] These authors contributed equally to this work.

[*] Authors to whom correspondence should be addressed.

E-mail Address: tskim1@kaist.ac.kr, jungyong.lee@kaist.ac.kr, jangwookchoi@kaist.ac.kr

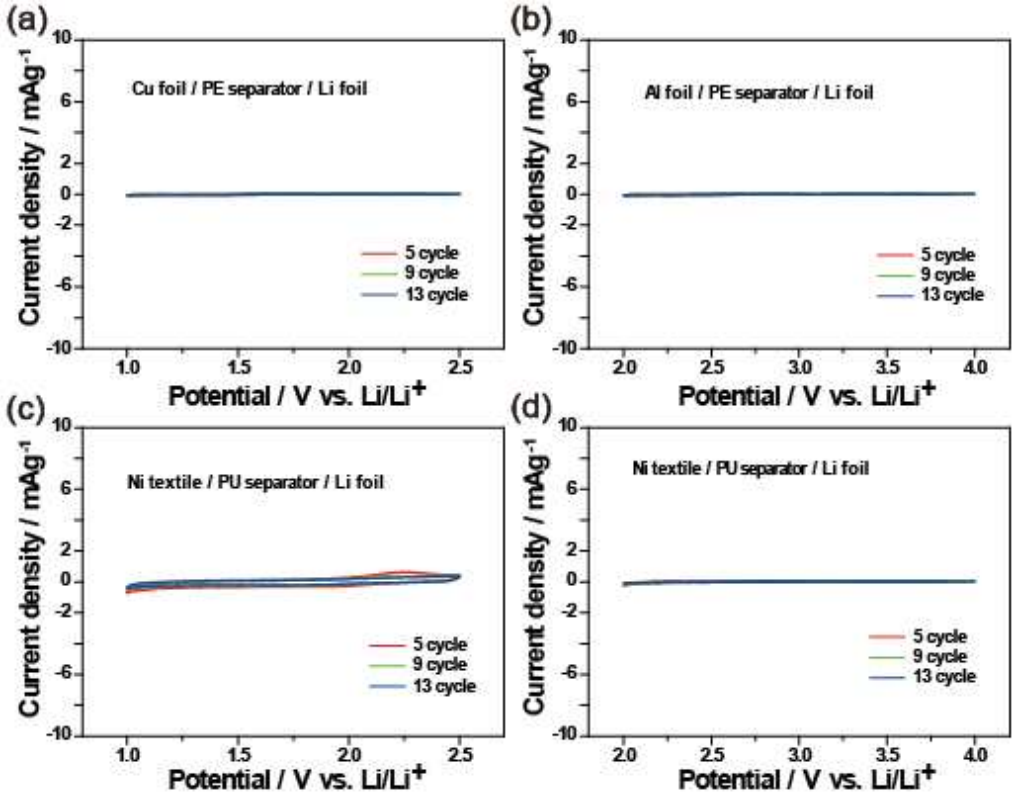

Figure S1. Electrochemical CV scans of current collectors. The CV scans at 0.1 mV s^{-1} of (a-b) the conventional foil-based batteries and (c-d) the textile-based batteries in the potential ranges of anodes (1.0~2.5 V vs. Li/Li^+) and cathodes (2.0~4.0 V vs. Li/Li^+).

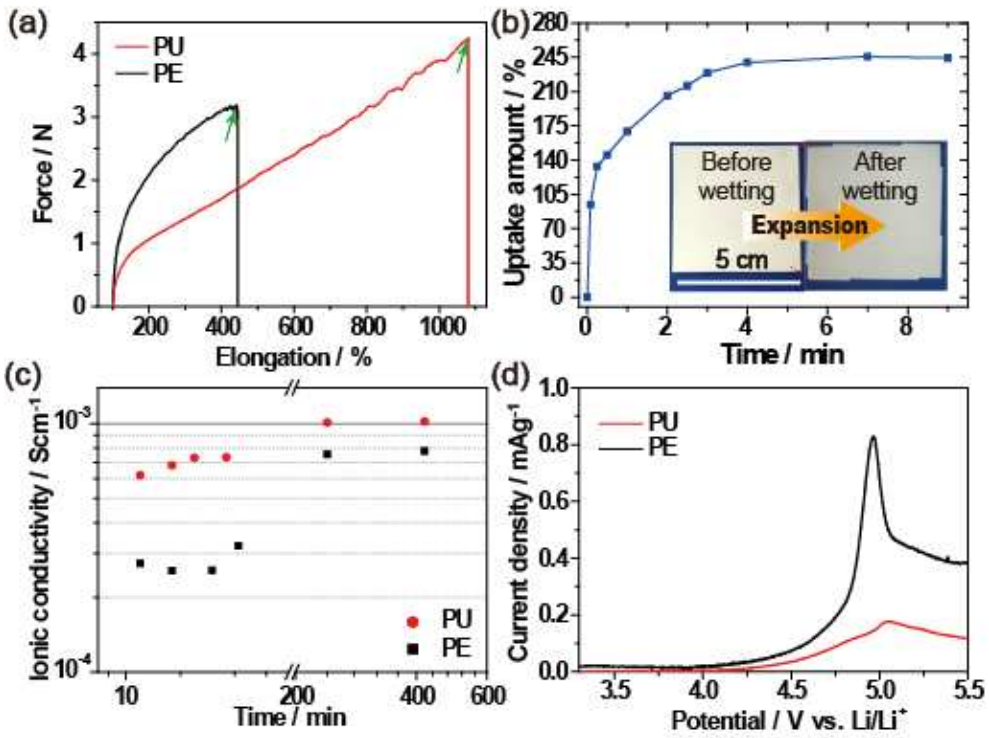

Figure S2. Characterization of the PU separator. (a) Force vs. elongation tests of the PU and PE separators. (b) The electrolyte uptake with the PU separator at different dipping times. For reference, the uptake amount was calculated based on $\frac{M2-M1}{M1} \times 100$, where $M1$ and $M2$ represent the weights of the separators before and after the dipping step. Also, such superior electrolyte uptake capability increases the dimensions of the PU separator by 9.76% in both horizontal and vertical directions upon complete absorption of the electrolyte. (c) The ionic conductivities of the PU and PE separators at various soaking times. The PU separator exhibits ~2.3 times higher ionic conductivity than those of the PE separator in the early soaking period of 12 min, but the values become close to each other after 240 min due to increased uptake amount of the PE separator. (d) A linear sweep voltammetry (LSV) curves for both separators in the potential range of 3.0~5.5 V vs. Li/Li^+ at a scan rate of 0.05 mV s^{-1}. The PU separator exhibits similar behavior to that of the PE separator with regard to electrolyte decomposition, implying that the PU separator is as electrochemically stable as the PE separator during the interaction with the commonly used electrolyte (1 M $LiPF_6$ in EC/DMC=1:1=v/v).

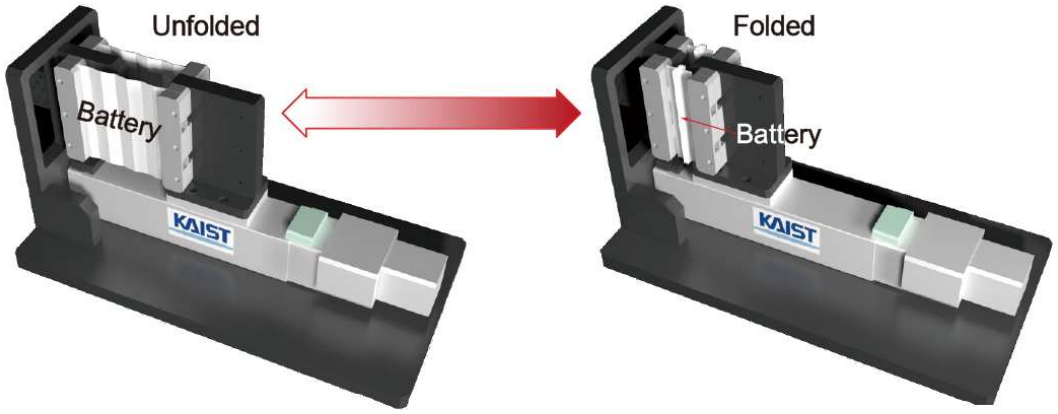

Figure S3. A schematic overview of the folding machine wherein the textile battery griped at both ends is repeatedly folded and unfolded during battery cycling.

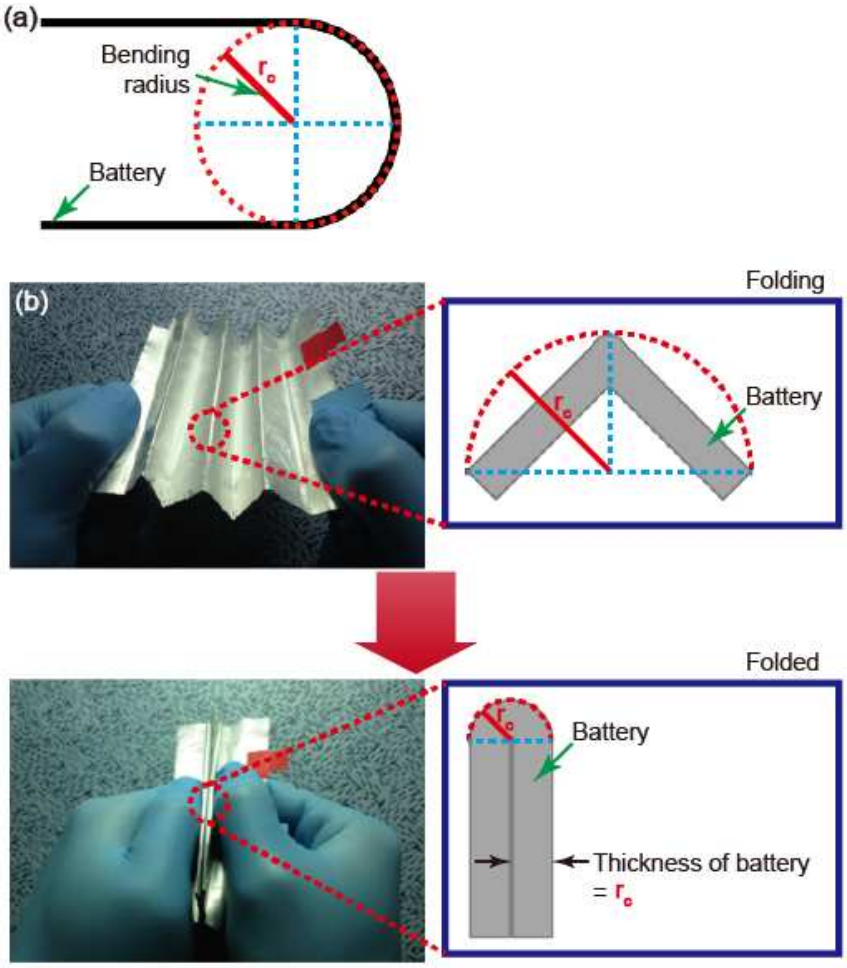

Figure S4. Bending radius of wearable textile battery. (a) The definition of the bending radius. (b) The bending radius changes during the folding motion.

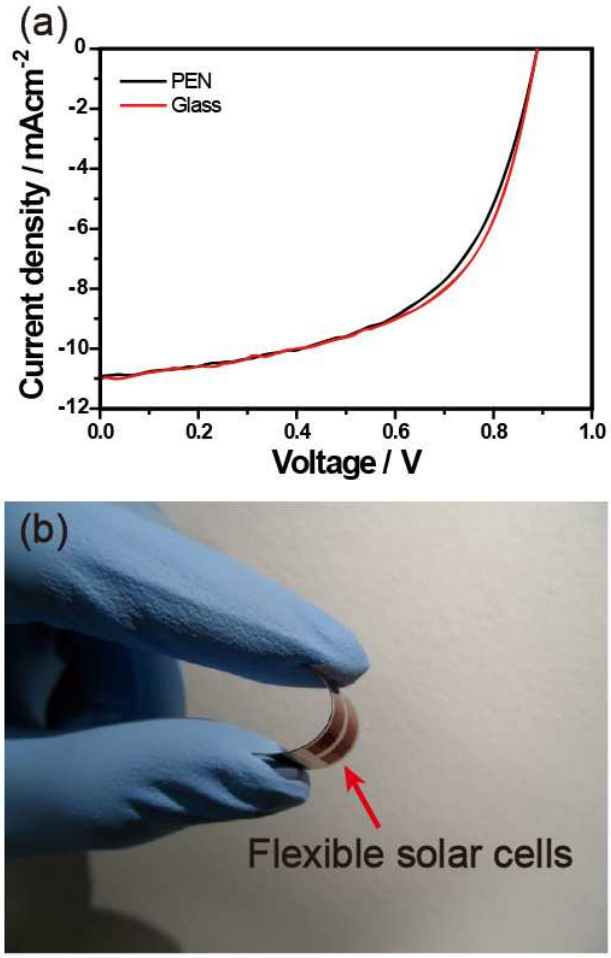

Figure S5. Polymer solar cells. (a) The current density-voltage (*J-V*) characteristics of polymer solar cells on a PEN substrate (black) and a glass substrate (red). The power conversion efficiency of the solar cells on the PEN and the glass substrates were 5.49% and 5.97%, respectively. (b) A photograph of flexible solar cells on a PEN substrate.

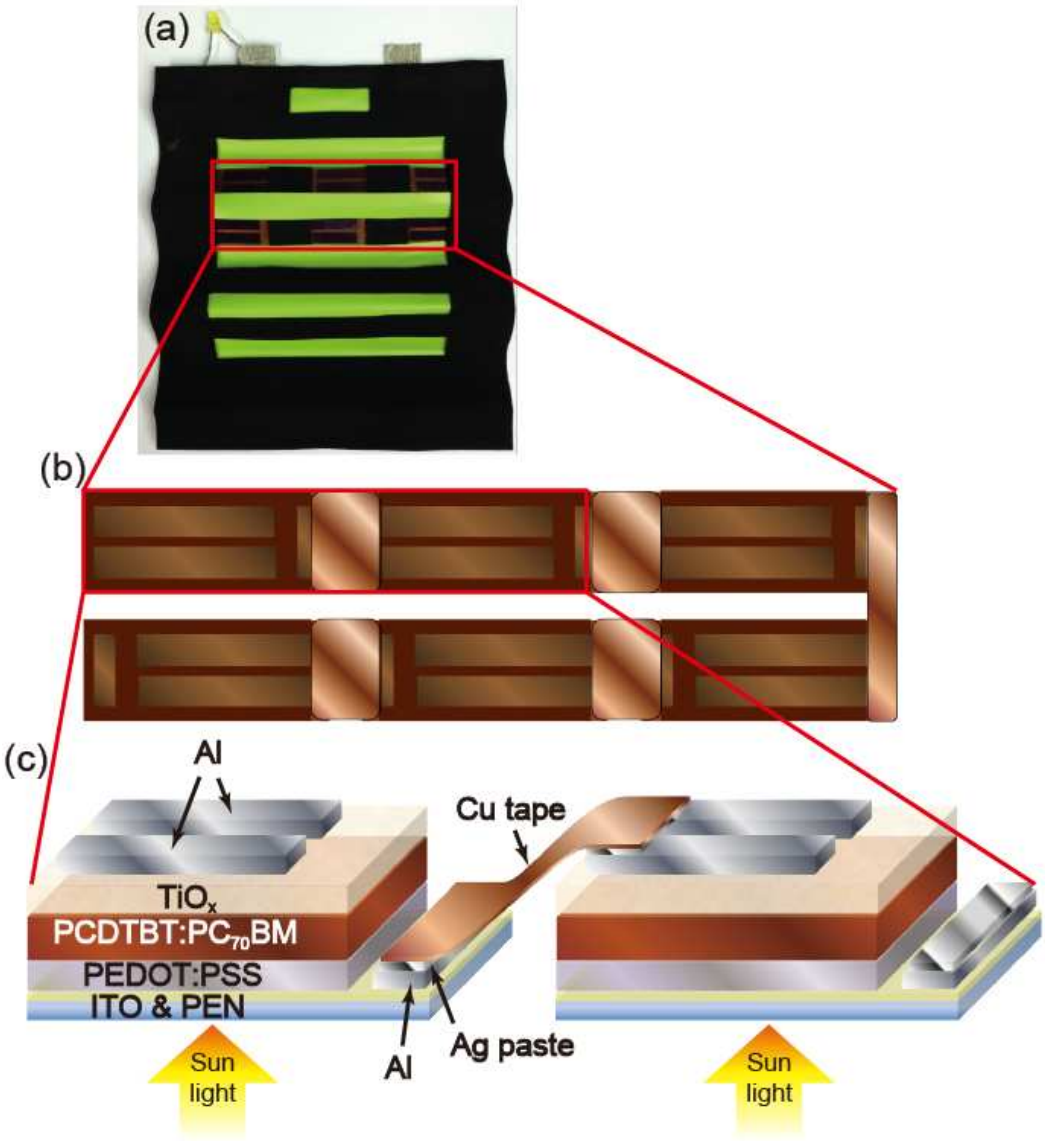

Figure S6. Wearable textile battery integrated with flexible solar cells. (a) A photograph of the wearable textile battery combined with flexible solar cells. (b) A schematic description showing that 6 solar cells are connected in series. (c) Detailed schematic of the connection between adjacent solar cells in the red box area of (b). The structure of the solar cell is PEN/ITO/PEDOT:PSS/PCDTBT:$PC_{70}BM$/TiO_x/Al. Cu tape coated with carbon connect the adjacent solar cells, and silver paste between the Cu tape and Al electrode enhances their adhesion.

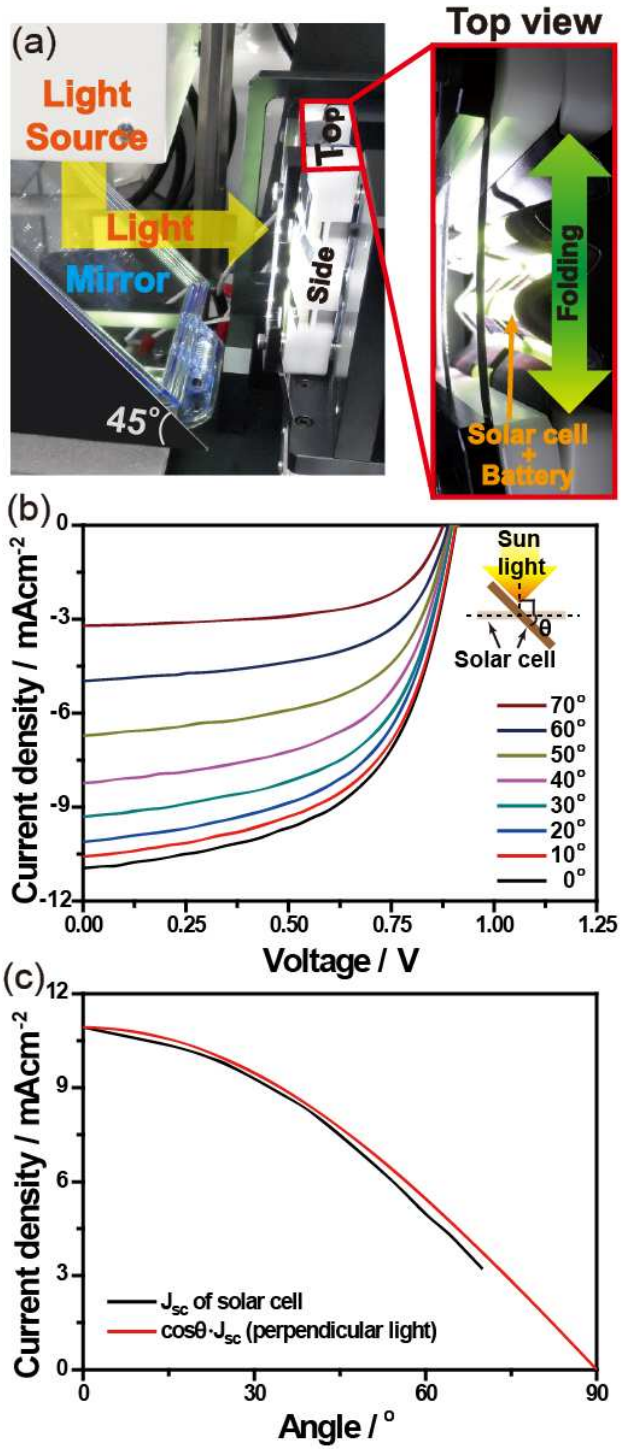
(a)
Light Source
Light
Mirror
45°
Top
Side
Top view
Folding
Solar cell + Battery
(b)
Current density / mAcm-2
Voltage / V
Sun light
θ
Solar cell
70°
60°
50°
40°
30°
20°
10°
0°
(c)
Current density / mAcm-2
Angle / °
Jsc of solar cell
cosθ·Jsc (perpendicular light)

Figure S7. Angular response of a polymer solar cell. (a) (Left) an instrumental setup for characterization of solar-charging capability during repeated folding-unfolding cycles. Due to the relative configuration of the folding machine and the solar simulator, the light was directed toward the textile battery using a mirror at a 45º angle. (Right) a top-view photograph indicating the folding direction. (b) *J-V* characteristics of polymer solar cells at various incident light angles. (c) Plots of measured short circuit current density (J_{sc}) of the solar cell as a function of incident light angle (black) and $\cos\theta \cdot J_{sc}$ (at normal incidence, red). They reveal that reduction of J_{sc} is due to the decreased light intensity from an oblique angle of incidence.

During the folding-unfolding cycle experiment as depicted in Supporting information Figure S7a, the angle of the battery surface ranges from 20º to 90º without a full stretch (0º). The time-averaged J_{sc} is calculated to be approx. 46.8% of the J_{sc} at normal incidence when the moving unit of the folding instrument translates at a constant speed. Considering reduced incident light intensity of 0.86 sun due to the mirror reflection (Supporting information Figure S7b), we estimated that the charging time of the wearable battery is stretched 2.48-fold, agreeing well with the actual potential profiles in a solar-charging mode, as illustrated in Figure 6c in the main text.

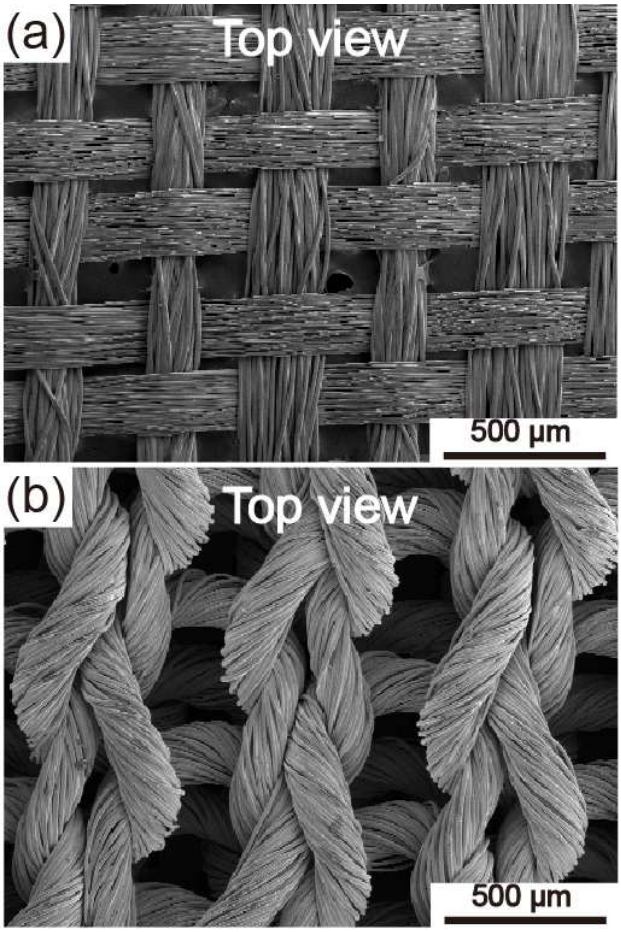

Figure S8. Top-viewed SEM images of the plane and the knitted textile. (a) The morphology of the plain textile and (b) the knitted textile after Ni coating. The thicknesses of both textiles are 85 and 450 μm, respectively.

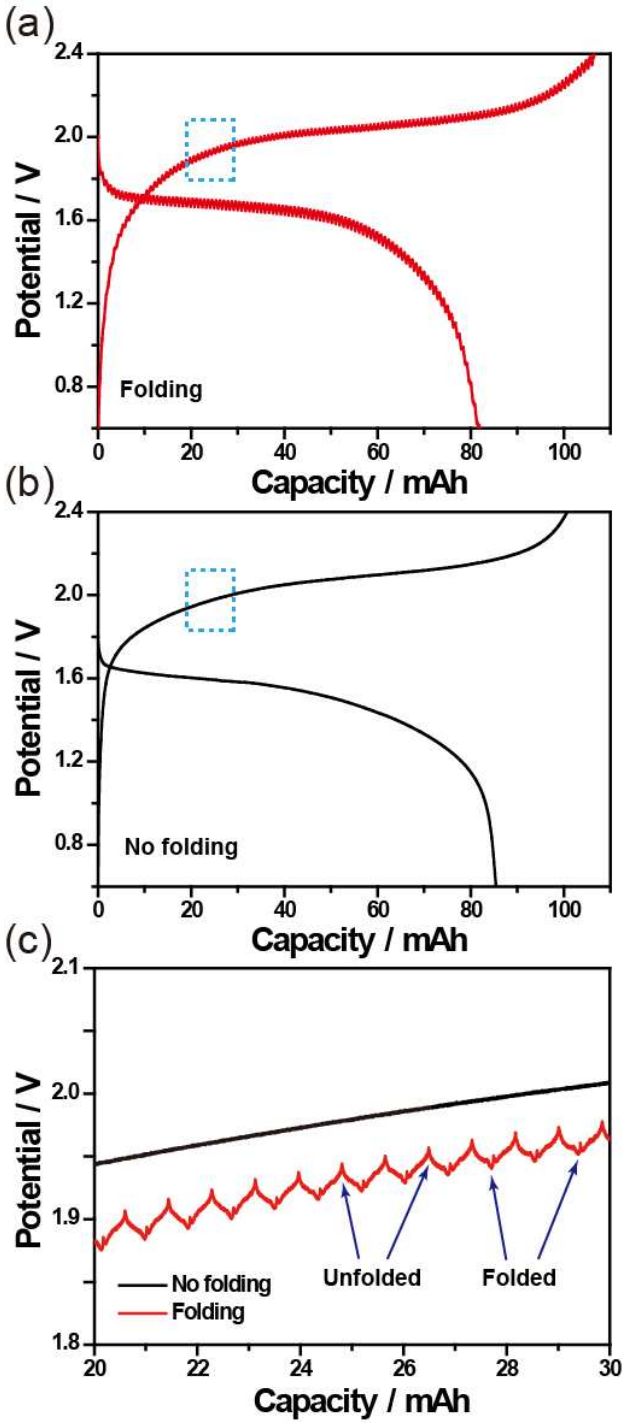

Figure S9. Electrochemical tests of the wearable textile battery with increased mass loading. The first cycle potential profiles (a) with and (b) without repeated folding-unfolding. (c) Magnified

charging profiles from the boxes in (a) and (b). The C-rates were 0.05C and 0.1C for (a) and (b), respectively. (a) and (b) are from separate cells: in the case of (a), the mass loadings of LFP and LTO are 712 and 889 mg for 5 x 5 cm^2, respectively. In this figure, the n/p ratio defined as actual total capacity ratio between anode and cathode is 1.08.

Movie S1. Contact angle test for the PE separator using the electrolyte.

Movie S2. Contact angle test for the PU separator using the electrolyte.

Movie S3. Mechanical folding-unfolding test by a home-built instrument. During the motions, the electrochemical performance was measured simultaneously.

Movie S4. Solar charging capability test while the mechanical folding-unfolding motions were engaged simultaneously. The light emitted from a solar simulator was under AM 1.5G illumination at 100 mW cm^{-2}.